J Radioanal Nucl Chem (2017) 312:19–28
DOI 10.1007/s10967-017-5206-1

Sorption of Cs and Sr radionuclides within natural carbonates

Pranesh Sengupta[1] · Jaishri Sanwal[2] · P. Mathi[3] · Jahur A. Mondal[3] · P. Mahadik[1] · N. Dudwadkar[4] · P. M. Gandhi[4]

Received: 27 September 2016 / Published online: 2 March 2017

Abstract Understanding the mobility of radiocesium and radiostrontium within geological environment is important from 'deep geological repository system'—safety assessment point of view. Cs and Sr radionuclide sorption studies have been carried out with a stalagmite sample collected from Lesser—Himalayas. Detailed microstructural studies, backed up by micro-Raman and LIBS analyses, identified three different domains within the sample; constituted of microcrystalline calcite, botryoidal aragonite and palisadic calcite respectively. Experimental studies showed that both the radionuclides exhibit moderate to low sorption coefficients within all the different domains of stalagmite under acidic environment.

Keywords Speleothem · Cs and Sr radionuclide · Sorption in natural carbonates · Nuclear waste disposal · Geological repository

Introduction

Isolation of high level nuclear waste (HLW) within 'multiple barrier system', is a widely accepted methodology for nuclear waste management [1, 2]. The idea involves fixing of HLW in suitable inert matrices and placing them inside deep geological repository within canisters/overpacks made up of stainless steel/copper alloy [3–15]. The metallic containers are isolated from host rock by composite layer of bentonite or other clay minerals, graphite, sand etc. [16–20]. Any openings remaining within the multi-barrier system are further blocked through backfilling with crushed rock, concrete, clay minerals etc. Both buffer and backfill materials provide cushioning effect to the metallic containers from external stresses. Countries like Finland, Sweden, Switzerland, France have already made significant progress in building geological repository system. Although such geological repositories are most likely to be constructed within dry regions but interaction between meteoric water with 'multiple barrier system' components cannot be ruled out. Such interactions become all the more important if one considers small local water bodies which are likely to form due to usage of water for construction and development of geological repositories. Creation of different openings such as boreholes, access shafts, galleries, disposal tunnels etc. will not only require significant amount of water but will also provide ample scopes for the construction materials (e.g. cement. cementitious backfill, plaster, grouted waste package etc.) and accumulated broken rock masses (due to excavation) to interact with flowing or stagnant water bodies. Needless to say, such natural and anthropogenic materials' interactions with water can lead to formation of cave-like carbonate deposits such as stalactite, stalagmites, columns, flowstones and draperies (collectively called speleothems) within geological repositories as has been witnessed within various man-made underground openings such as abandoned road tunnels, water channels, mines etc. [21–33]. It is therefore understood that such carbonate precipitations within geological repository or adjacent to any nuclear

✉ Pranesh Sengupta
sengupta@barc.gov.in

[1] Materials Science Division, Bhabha Atomic Research Centre, Mumbai 400 085, India

[2] Geodynamics Unit, Jawaharlal Nehru Centre for Advanced Scientific Research, Bangalore 560064, India

[3] Radiation & Photochemistry Division, Bhabha Atomic Research Centre, Mumbai 400 085, India

[4] Fuel Reprocessing Division, Bhabha Atomic Research Centre, Mumbai 400 085, India

facility, can modify fluid flow-paths through altering rock porosity and permeability, which may ultimately result in facilitating (creation of open spaces through dissolution) or isolating (immobilization through sorption and/or co-precipitation) radionuclides from contacting with the mobile fluid phase [34–37]. Such reduction in narrow open spaces due to precipitation can also hinder maintenance of homogeneous chemical/radiochemical/thermal/microbial environment within geological repositories.

The possibility of radionuclide migrations and redistributions within geological repository arise in the event of failure(s) of 'Engineered Barrier Systems (EBS)' i.e. canister, overpack and buffer materials. In such event, the HLW waste matrix can come in contact with water and through its leaching the radionuclides can get released into 'near field region'. Of the various components, Cs (cesium) and Sr (strontium) radionuclides, particularly ^{137}Cs (half life $\sim$30 years) and ^{90}Sr (half life $\sim$28.8 years) are important as they are known to be (i) major heat producing radionuclides, (ii) abundant within HLW, (iii) relatively easily leachable from waste form matrices, and (iv) emit γ-rays and β-particles respectively. Among the other Cs radionuclides ^{135}Cs has a long half-life ($\sim 2\times10^6$ years) also. Because of their high solubility within ground waters; as Cs^+ and Sr^{2+} under all conditions of Eh and pH; and sorption within natural materials, radiocesium and radiostrontium can become part of food chain web which can significantly affect health and safety of biosphere [38–40]. For example, substitution of ^{90}Sr for Ca in human bone can lead to irradiation of bone marrow thereby increasing the chance of leukaemia [41]. It may be mentioned here that calcium carbonates being one of the major constituents of Earth's crust, play a major role in the preservation of biosphere and food-chain web through regulating 'carbon cycle'. Calcium carbonates get precipitated from solvated calcium and carbonate ions as a result of supersaturation or as a biomineralization product. Apart from geological repository scenario, radiocesium and radiostrontium can encounter carbonate materials in the event of approved release, accidents/fall outs [42–44] or leakage of HLW-storage tanks as happened in Hanford, USA [45–47], Oak Ridge, USA [48, 49], Sellafield, UK [50] and Mayak, Russia [51, 52]. Incorporation radiocesium and radiostrontium within natural rocks (mostly of sedimentary origin), soils and minerals take place due to multi-site sorption. Experimental studies have shown that these radionuclides get preferentially fixed at 'Frayed Edge Sites' or sorped on 'Regular Exchange Complex Sites' like interplanar sites or edge lattice positions [53–59]. Needless to say, considering the prolong service period of geological repository ($\sim$one million years) it is very important to develop sorption database for important radionuclides on all possible natural materials that are likely to be encountered within multiple barrier system. This will help in 'total system performance assessments' as well as to carry out modeling study [60]. Unfortunately no sorption studies have been carried out for radiocesium and radiostrontium on naturally precipitated carbonate materials. In order to fill-up this gap, an attempt has been made in the present investigation to understand the sorption of Cs and Sr radionuclides on natural carbonates, using stalagmite sample collected from Dharamjali cave (Pithoragarh district) in the eastern Kumaun Lesser Himalaya [61]. Details of the experimental procedures are given below.

Experimental

For the present study, stalagmite samples were collected from Dharamjali cave occurring within Thalkedar limestone of Kumaun Lesser Himalaya. A representative stalagmite sample from Dharamjali cave and its cross-section is shown in (Fig. 1). The sample has been characterized for its physical and chemical properties before it was taken for radiochemical sorption studies.

Physical characterization

Phase analysis of the stalagmite sample has been carried out using optical microscopic technique. Thin slices of the stalagmite were mounted on glass slides, ground on different grades of emery papers and finally polished on lapping wheel using 0.5 μm diamond paste.

Same polished samples were used for phase analyses (at ambient temperature and pressure) using micro-Raman spectroscopy. The analyses spots were excited at 532 nm (Nd-YAG laser; power $\sim$20 mW at sample position) using a 10× objective lens. The scattered light was collected by the same objective lens and passed through an edge filter to separate the Stokes signal from the Rayleigh and anti-Stokes scattered signals. The Stokes signal after the edge filter was passed through a fiber-coupled spectrograph (Acton series SP 2300i, 1800 groove/mm) and detected by a thermo-electric cooled (−75 °C) charge-coupled device (CCD). The resolution of instrument was 1 cm^{-1}.

Chemical characterization

In line with the focus of present study, trace elemental analysis of stalagmite samples has been carried out using a non-destructive spectroscopic method called 'laser induced breakdown spectrometry (LIBS)'. It involved ablating a small quantity of the sample and monitoring the subsequent emission from atomic species. To this end, a 50 fs Ti–Sapphire laser system ($\lambda = 800$ nm) operating at 1 kHz was employed to generate plasma by focusing 1 mJ of

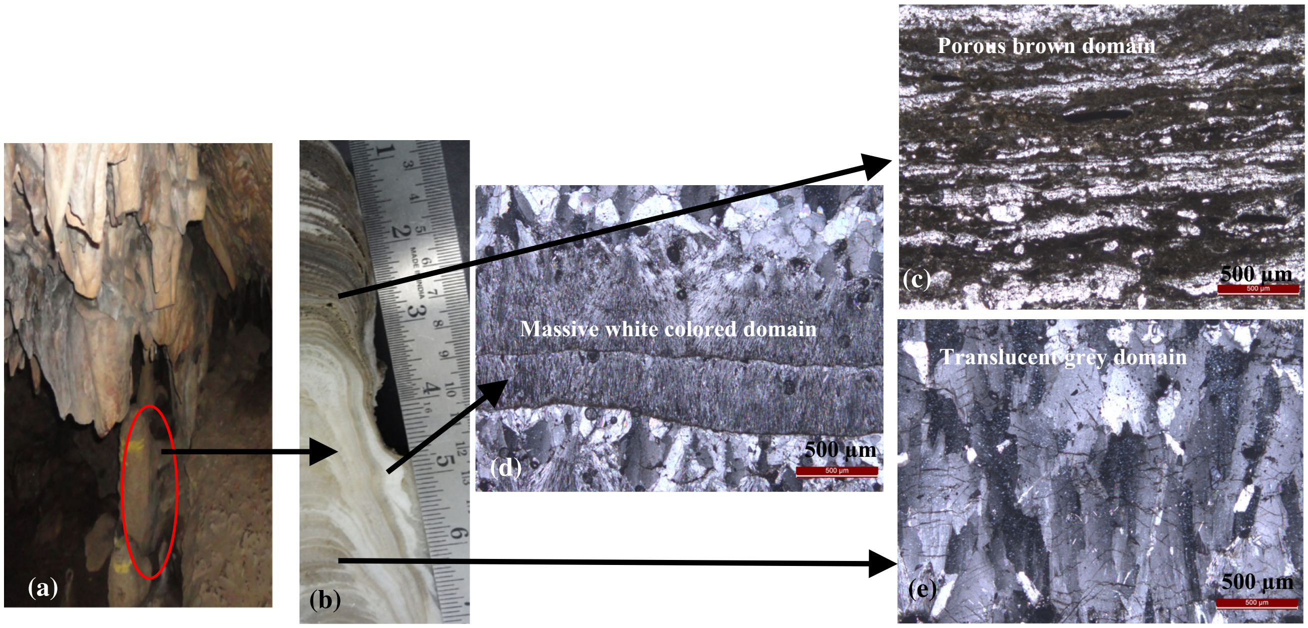

Fig. 1 Cross-section of **a** the natural stalagmite is shown in **b**. Note the optical images of three major domains **a** coarse columnar calcite crystals within translucent layer, **b** microcrystalline calcite interlayered with unidentified *brownish/greyish* phase(s) within *grey layers*, and **c** botryoidal fibrous aragonite crystals defining the *milky white layers*. (Color figure online)

energy onto the sample surface using a BK7 planoconvex lens ($f = 10$ cm) to a spot diameter of approximately 14 µm. The samples were mounted on a motorized Y–Z translational stage so as to provide a fresh surface for each laser shot and thereby obtain compositional profiles across different domains. An Echelle grating spectrograph in conjunction with an ICDD (International Centre for Diffraction Data) is used for acquisition of spectra.

Radionuclide sorption study

For present experimental study, ^{137}Cs and $^{85+89}$Sr radiotracers were extracted from HLW arising from PUREX process and purified by cation exchange route [62]. To ensure better quality of data, experimental parameters were optimized following the procedure outlined in Sanwal et al. [33].

Following batch equilibration, ^{137}Cs and $^{85+89}$Sr sorption experiments were carried out with vortex shaker. Powdered samples (0.1 g) were added to solutions (3 mL), each of which were spiked separately with ^{137}Cs and $^{85+89}$Sr and maintained at fixed pH (1–6). Equilibration time was maintained at 60 min for each study. After the experiments, solutions were filtered and counted using single channel gamma analyzer equipped with NaI(Tl) detector. For better accuracy, separate examinations were done with blank solutions and tracer absorption on the walls of extraction vials were found negligible. K_d (distribution coefficients), were calculated using following equation:

$$K_{\rm d} = [V(C_o - C_e)]/C_e \times M \quad (1)$$

where 'C_o' and 'C_e' are feed and effluent concentrations respectively; 'V' is volume (mL) of solution, and 'M' is amount of ion exchanger/adsorbent used.

It may be mentioned here that the requirement for carrying out the present sorption study under acidic pH stems out for two reasons. (i) Presence of localized acidic environment, within repository or any other geological environment with nuclear facilities, due to presence of fulvic acids and humic substances cannot be ruled out [63–75], and (ii) earlier experimental studies show natural carbonates (calcite and aragonite) may not totally dissolve even under strong acidic environment [32, 33]. This observation is contradictory to common belief but the possible reasons of enhancement of natural carbonate stability even under acidic conditions are being evaluated separately. One possible reason could be natural incorporation of wide range of trace elements within carbonate lattices [76–79].

Results and discussion

Physical characterization

Longitudinal cross section of the natural stalagmite sample (Fig. 1a) is shown in Fig. 1. It is evident from Fig. 1b that the sample has three basic components, namely (i) porous brown colored domains, (ii) massive white domain, and (iii) translucent grey colored domains. Representative optical images of the three components are given in Fig. 1c–e. As evident from Fig. 1c, the porous domain is found to be very thinly layered, fine grained and highly pitted. High magnification optical images identify the domain as made up of microcrystalline calcite. On the other hand, white domain is found to be constituted of botryoidal aragonite needles (Fig. 1d). The remaining translucent domain is constituted of elongated calcite phases, commonly known as 'palisadic' type.

The interpretations of the optical microscopic images (Fig. 1) to different microcrystalline phases have been verified with micro-Raman data (Fig. 2). Although the calcite, aragonite and ikaite have overlapping Raman bands, their specific occurrences were indicated by certain characteristic peaks. For example, in the low frequency region, the Raman band at 207 cm^{-1} is characteristics of aragonite/ikaite structures whereas that at 282 cm^{-1} is the manifestation of calcite as well as aragonite structures [80]. Moreover, the in-plane bending mode of aragonite appears at 705 cm^{-1} and shift to higher frequency (at 712 cm^{-1}) for calcite [81]. Figure 2 shows the Raman spectra of the stalagmite sample corresponding to the three distinctly coloured domains, (i) white (ii) brown and (iii) grey. As shown in the top panel of Fig. 2, the Raman spectrum of the brown and grey colored domains are almost identical to each other while that at the white domain is different. The spectral bands corresponding to different vibrational modes of the stalagmite sample are shown in expanded form in the bottom panels of Fig. 2. The white domain of stalagmite sample shows multiple bands in the low frequency region (154, 183, 207 and 260 cm^{-1}) but the brown and grey domains show only two bands (158 and 283 cm^{-1}; bottom left panel in Fig. 2). Thus, the white domain contains aragonite and/or ikaite structures, and the brown/grey domains contain calcite and/or aragonite structures [80, 81]. Expanded view of the second higher energy band (in-plane bend of CO_3^{2-}) shows that the band appears at 704 cm^{-1} for the 'white domain' and shifts to 712 cm^{-1} for the brown/grey domains' (bottom middle panel in Fig. 2), which is a clear signature that the white domain is rich in aragonite and the brown/grey domain in calcite. Moreover, the position of the symmetric stretch band of CO_3^{2-}, which can distinguish between ikaite (1070 cm^{-1}) and aragonite/calcite (1086 cm^{-1}) structures, appears at 1087 ± 2 cm^{-1} for all the three domains (white, brown and grey) of the stalagmite sample. Thus, the position of the CO_3^{2-}-symmetric stretch band, in agreement with the position of the in-plane bending of CO_3^{2-}, conclusively proves that white domain of the sample is rich in aragonite and the brown/grey regions in calcite.

Chemical characterization

Certain elements (e.g. Sr, Mg, Rb etc.) which are present within HLW are also known to occur within natural fluids which lead to precipitation of natural carbonates. It is therefore always interesting to know of this gamut of available cations and anions, which are the ones which get fixed within the carbonate lattices and how their respective compositional variation relates to phase changes which happen within speleothem in micrometer to few millimetre scales mostly due to fluctuations in climate. This

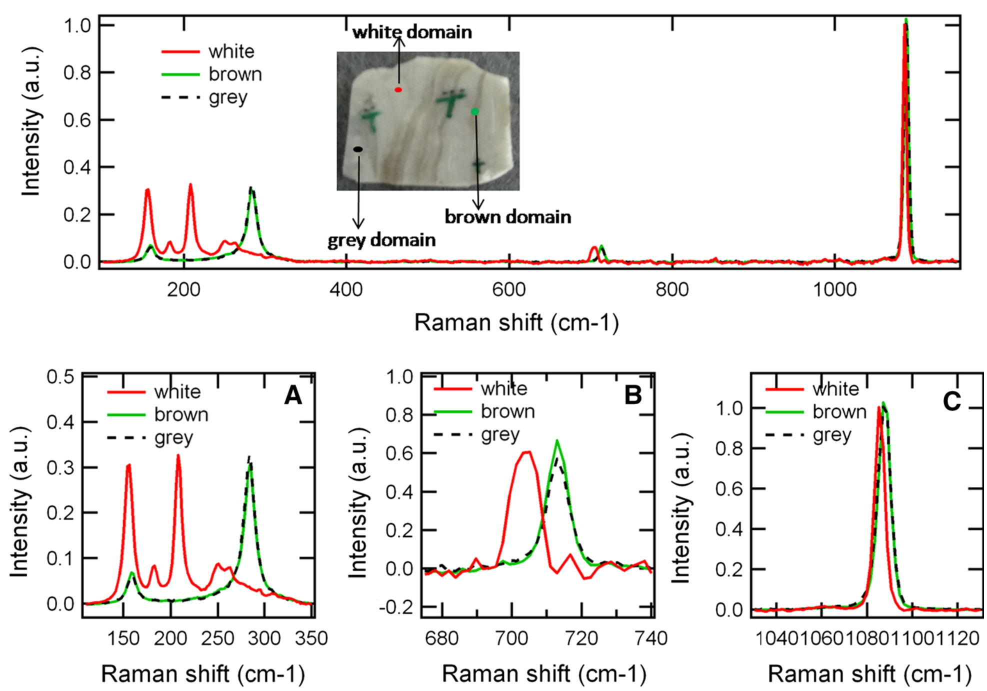

Fig. 2 *Top panel*: Raman spectrum of polished stalagmite in three different regions (*white*, *brown* and *grey*). The picture of the sample is shown in the *inset*. *Bottom panels*: expanded view of the different vibrational bands: lattice vibration (*left*), CO_3^{2-} in-plane bend regions (*middle*) and CO_3^{2-} symmetric stretch (*right*). (Color figure online)

information is important to explain sorption experimental data as well. Representative LIBS data are shown in Fig. 3. It is noted that the brown domain constituted of microcrystalline calcite contained significant amount of K (potassium) whereas Mg (magnesium) was preferentially locked inside columnar calcite rich grey domains. Sr (Strontium) exhibited higher preference for aragonite containing white domains. Similar trace elements distribution trends, in terms of Sr/Ca and Mg/Ca ratios, are observed across the multiple layers of the stalagmite (Fig. 4). What becomes very clear from this study are, in case of an open system where different calcium carbonates are allowed to precipitate from natural liquid, (a) among the calcium carbonates Sr has a preference for aragonite over calcite, and (b) aragonite can host Sr over long time scale.

Radionuclide sorption study

Sequestration of radionuclides within geological repositories by natural carbonates will be primarily done by sorption mechanisms especially at the initial stages. The sorption mechanism may involve various processes in operation, either individually or collectively like

- adsorption (building up of chemical component at the fluid/solid interfaces without formation of a three dimensional molecular arrangement),
- absorption (uptake of a (fluid) chemical component within micro/nanoporous solid (e.g. in zeolites) through diffusion),
- precipitation (incorporation of an aqueous chemical component within a given solid phase through growing (homogeneous/heterogeneous nucleation) a three dimensional crystalline molecular arrangement,
- co-precipitation (precipitation process involving specific trace element iso-structural with one of the host component), and
- recrystallization (reconstitution of host's crystalline structure to a similar one but with different trace element concentrations as a function of intensive/extensive variables of the system).

Over prolonged time-scale of interaction, all these processes can operate in the following sequence (arranged in order of increasing reaction time durations), adsorption → absorption → precipitation → co precipitation → recrystallization. The present experimental study

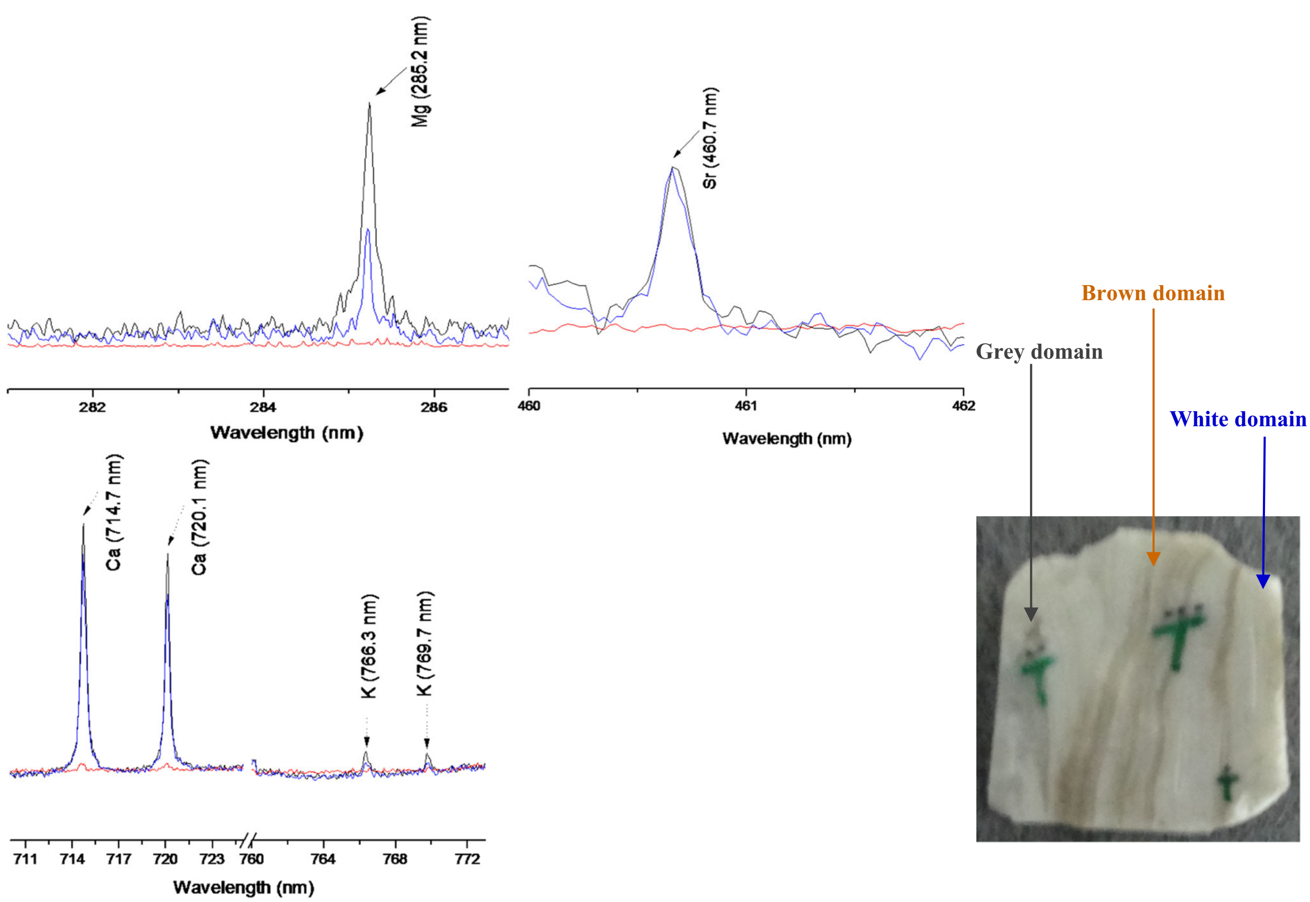

Fig. 3 LIBS data from different domains of stalagmite

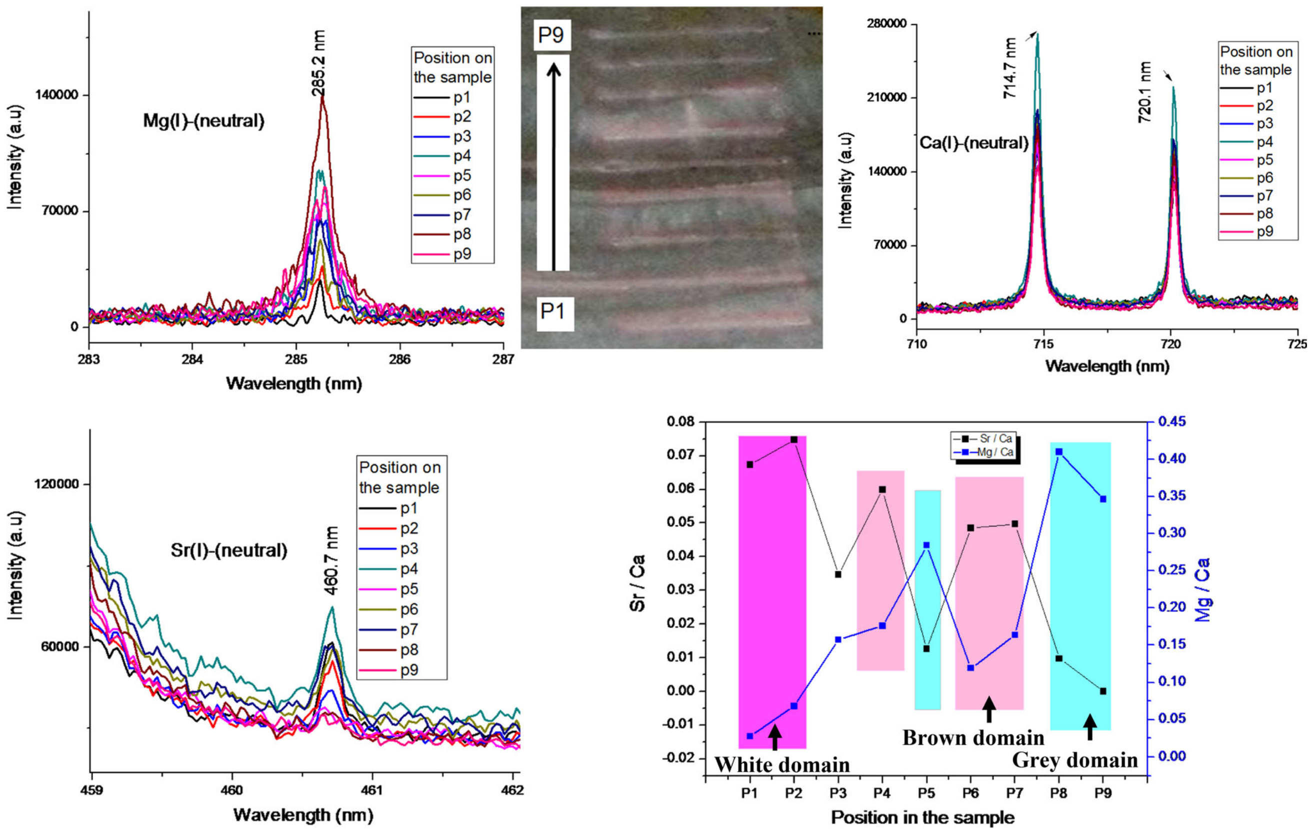

Fig. 4 Elemental distributions in different domains of stalagmite

however corresponds to the faster sorption mechanism only i.e. adsorption process.

Detail experimental results for sorption studies are given in Tables 1 and 2. To optimise 'equilibration time', experiments with powdered carbonate domains were carried out over a time interval ranging from 5 to 60 min [32, 33]. In order to remove any possible perturbations in sorption kinetics due to 'nucleation and crystal growth mechanisms [82]', higher contact time was avoided. As sorption was maximum at 60 min so this was considered as equilibration time duration. Keeping equilibration (contact) time fixed at 60 min, centrifugation speed was optimized and high %sorption values were obtained for 7000–8000 rpm [32, 33]. Hence, all other experimental studies were done maintaining centrifugation speed at 8000 rpm. Similarly, in 'volume efficiency' experiments (with 5–20 mL feed solutions) maximum K_d value was obtained for 5 mL solution [32, 33].

For all studied radionuclides, sorption coefficients within different domains of stalagmite are found to be

Table 1 ^{137}Cs sorption studies (5 mL of feed solution with initial concentration, C_o = 280.20 mCi/L; equilibration time: 60 min with vortex shaker) [%Sorption = $(C_o - C_e) \times 100/C_o$, $K_d = (C_o - C_e) \times V / (C_e \times M)$]) on 0.05 g (=$M$) powdered aragonite, columnar calcite and microcrystalline calcite domains over pH range of 1–6. Δ aragonite, ○ columnar calcite, □ microcrystalline calcite domains

pH	Effluent concentration (μCi/L) C_e			%Sorption			Decontamination factor (C_0/C_e)			K_d (mL/g)		
	Δ	○	□	Δ	○	□	Δ	○	□	Δ	○	□
1	2446	2846	3627	99	98	76	114	98	77	1237	9732	7619
2	2000	2290	3012	99	99	99	140	122	93	6955	12,136	9209
3	2003	2003	2836	99	99	99	140	139	98	13,889	13,910	9766
4	1736	1936	2682	99	99	99	161	144	104	16,340	14,343	10,355
5	1643	1843	2498	99	99	99	170	152	112	17,055	15,128	11,108
6	1512	1712	1963	99	99	99	185	163	142	18,431	16,286	14,196

Table 2 $^{85+89}Sr$ sorption studies (5 mL of feed solution with initial concentration, $C_o = 980.29$ µCi/L; equilibration time: 60 min with vortex shaker) [%Sorption = $(C_o - C_e) \times 100/C_o$, $K_d = (C_o - C_e) \times V/(C_e \times M)$]) on 0.05 g (=$M$) powdered aragonite, columnar calcite and microcrystalline calcite domains over pH range of 1–6. Δ aragonite, ○ columnar calcite, □ microcrystalline calcite domains

pH	Effluent concentration (µCi/L) C_e			%Sorption			Decontamination factor (C_0/C_e)			K_d (mL/g)		
	Δ	○	□	Δ	○	□	Δ	○	□	Δ	○	□
1	190	290	350	86	70	64	5	3	2	414	237	180
2	174	191	299	98	98	69	5	6	3	462	412	227
3	152	164	252	93	93	74	6	6	4	554	497	289
4	133	124	233	95	95	76	7	8	4	635	689	320
5	102	90	111	93	93	89	9	10	9	856	984	857
6	102	72	99	98	97	89	9	13	10	860	1261	887

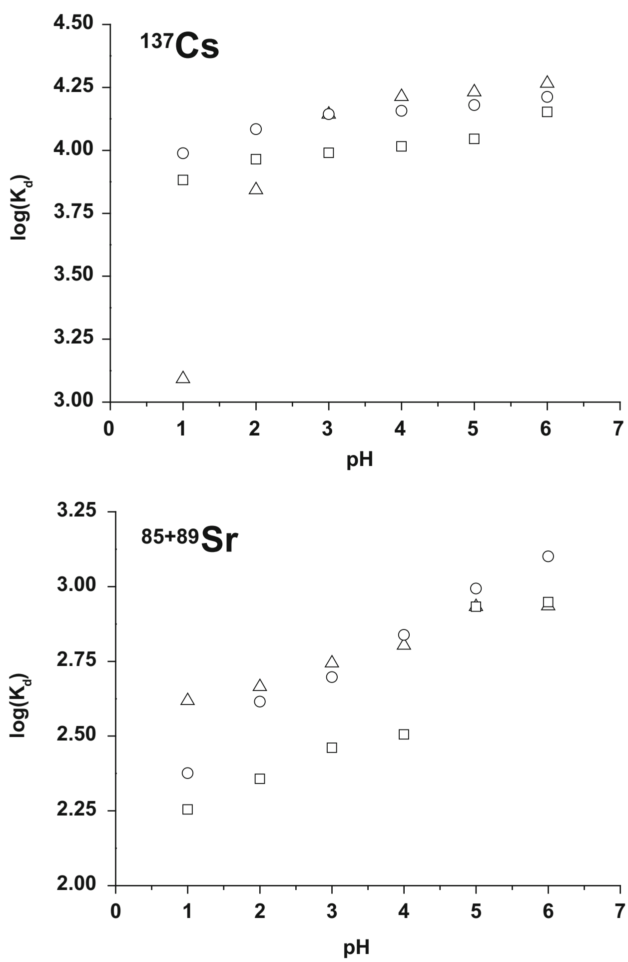

Fig. 5 Variations in log(K_d) values of ^{137}Cs, and ^{90}Sr within different phases of cave deposits (Δ aragonite, ○ columnar calcite, □ microcrystalline calcite) as a function of pH

from moderate to low. ^{137}Cs sorption was found higher in calcite (both columnar and microcrystalline varieties) compared to aragonite at low pH (1–2) and it reversed with increasing pH (Fig. 5a). Similar was the trend for $^{85+89}Sr$ (Fig. 5b) also, but the K_d value was much less compared to those for Cs-sorption. This observation comes as a contradiction to the general perception that sorption of Sr radionuclides should be more on calcium carbonate surfaces than Cs due to similarity in ionic charges. The reason behind such contradictory observations is being explored in the light of present simulation studies. One possible reason behind lower sorption K_d of radiostrontium, in comparison with that of radiocesium, may be due to already existence of Sr within active sorption sites of speleothems domains (incorporated during its formation through natural process), which might have acted as barrier towards further sorption of similar elements. In fact the present LIBS data show higher abundance of Sr within aragonite domains compared to calcite ones. But it may also be mentioned here that in actual scenario radionuclide sorption depends on various factors including crystal chemistry of substrate [83], fluctuations in solution chemistry (steady state vs non-steady state [84], dominant speciation on carbonate surfaces [85] etc. In fact recent leaching studies with thermodynamically most stable surface plane of calcite (104) show existence of equilibrium dynamics between dissolution and re-precipitation with strong control over recrystallization by pH, CO_2 partial pressure, and presence of ions in the aqueous phase [86].

Conclusions

Detailed microstructural studies of stalagmite sample revealed presence of three parts, namely (i) porous brown colored domains, (ii) massive white domains, and (iii) translucent grey colored domains. Optical microscopic analyses of the domains identified them to made up of microcrystalline calcite (brown domain), botryoidal aragonite (white domain) and palisadic calcite (grey domain) respectively. Phase identifications of the domains were further confirmed by micro-Raman analyses. Since calcite, aragonite and ikaite have overlapping Raman bands, so their presence were identified by certain characteristic peaks/spectral bands occurring in the low and high frequency regions, in-plane bending modes, vibrational modes and symmetric stretch band of CO_3^{2-}.

Trace-elemental analyses using LIBS technique showed that microcrystalline calcite domains were rich in potassium (K) whereas magnesium (Mg) was more in palisadic calcite domains. Strontium exhibited higher preference for aragonite domains. It became apparent from this study that Sr has a preference for aragonite over calcite.

Detail experimental results from sorption studies show that both the radionuclides exhibit moderate to low sorption coefficients within all the different domains of stalagmite. Sorption of ^{137}Cs and $^{85+89}$Sr was more in calcite (both columnar and microcrystalline varieties) compared to aragonite at low pH (1–2) and it reversed with increasing pH. Interestingly K_d values for $^{85+89}$Sr was much less compared to those for Cs-sorption. One possible reason behind this could be pre-existence of Sr within active sorption sites (as evidenced from LIBS data) in course of natural growth of speleothem that inhibited further incorporation of similar element within carbonate lattices under acidic environment.

Acknowledgements Authors thank Dr. G.K. Dey, Associate Director, Materials Group, BARC, Dr. Ajay K Singh, RPCD, BARC and Prof. K.S. Valdiya, Prof. B.S. Kotlia, Prof. C.P. Rajendran and Prof. Kusala Rajendran for their support. Two anonymous reviewers and Handling Editor are profusely thanked for their very valuable and constructive suggestions. The work was funded by Department of Atomic Energy, Government of India. JS acknowledges DST SERC Fast Track Scheme (No. SR/FTP/ES-97/2009) for financial assistances.

References

1. Donald IW (2010) Waste immobilization in glass and ceramic based hosts. Wiely, Hoboken, p 493
2. Ojovan MI, Lee WE (2005) An introduction to nuclear waste immobilization. Elsevier, Amsterdam, p 315
3. Sengupta P (2012) A review on immobilization of phosphate rich high level nuclear wastes within glass matrix—present status and future challenges. J Hazard Mater 235–236:17–28
4. Sengupta P, Fanara S, Chakraborty S (2011) Preliminary study on calcium aluminosilicate glass as a potential host matrix for radioactive ^{90}Sr—an approach based on natural analogue study. J Hazard Mater 190:229–239
5. Sengupta P, Kaushik CP, Dey GK (2013) Immobilization of high level nuclear wastes: the Indian Scenario. In: Ramkumar M (ed) On a Sustainable Future of the Earth's Natural Resources. Springer, Berlin, pp 25–51 **ISBN: 978-3-642-32916-6, 2013**
6. Sengupta P, Dey KK, Halder R, Ajithkumar TG, Abraham G, Mishra RK, Kaushik CP, Dey GK (2015) Vanadium in borosilicate glass. J Am Ceram Soc 98:88–96
7. Mishra RK, Sudarsan V, Sengupta P, Vatsa RK, Tyagi AK, Kaushik CP, Das D, Raj K (2008) Role of sulphate in structural modifications of sodium barium borosilicate glasses developed for nuclear waste immobilization. J Am Ceram Soc 91:3903–3907
8. Mishra RK, Sengupta P, Kaushik CP, Tyagi AK, Kale GB, Raj K (2007) Studies on immobilization of thorium in barium borosilicate glass. J Nucl Mater 360:143–150
9. Das N, Sengupta P, Roychowdhury S, Sharma G, Gawde PS, Arya A, Kain V, Kulkarni UD, Chakravartty JK, Dey GK (2012) Metallurgical characterizations of Fe–Cr–Ni–Zr base alloys developed for geological disposal of radioactive hulls. J Nucl Mater 420:559–574
10. Grover V, Sengupta P, Bhanumurthy K, Tyagi AK (2006) Electron probe microanalysis (EPMA) investigations in the CeO_2–ThO_2–ZrO_2 system. J Nucl Mater 350:169–172
11. Jafar M, Sengupta P, Achary SN, Tyagi AK (2014) Structural and phase evolution studies in $CaZrTi_2O_7$–$Nd_2Ti_2O_7$ systems. J Am Ceram Soc 97:609–616
12. Jafar M, Sengupta P, Achary SN, Tyagi AK (2014) Phase evolution and microstructural studies in $CaZrTi_2O_7$ (zirconolite)-$Sm_2Ti_2O_7$ (pyrochlore) system. J Euro Ceram Soc 34:4373–4381
13. Sengupta P, Rogalla D, Becker HW, Dey GK, Chakraborty S (2011) Development of graded Ni-YSZ composite coating on Alloy 690 by Pulsed Laser Deposition technique to reduce hazardous metallic nuclear waste inventory. J Hazard Mater 192:208–221
14. Sengupta P, Kaushik CP, Mishra RK, Kale GB (2007) Microstructural characterization and role of glassy layer developed on Inconel 690 during a nuclear high-level waste vitrification process. J Am Ceram Soc 90:3057–3062
15. Sengupta P, Kaushik CP, Kale GB, Das D, Raj K, Sharma BP (2009) Evaluation of alloy 690 process pot at the contact with borosilicate melt pool during vitrification of high level nuclear waste. J Nucl Mater 392:379–385
16. Ejeckam RB, Sherriff BL (2005) A ^{133}Cs, ^{29}Si, and ^{27}Al MAS NMR spectroscopic study of Cs adsorption by clay minerals: implications for the disposal of nuclear wastes. Can Miner 43:1131–1140
17. Kroupova H, Stamberg K (2005) Experimental study and mathematical modeling of Cs(I) and Sr(II) sorption on bentonite as barrier material in deep geological repository. Acta Geodyn Geomater 2:79–86
18. Yildiz B, Erten HN, Kis M (2011) The sorption behavior of Cs^+ ion on clay minerals and zeolite in radioactive waste management: sorption kinetics and thermodynamics. J Radioanal Nucl Chem 288:475–483
19. Mukhopadhyay J, Sengupta P, Tyagi AK (2015) Uptake of Cs and Sr radionuclides within oleic acid coated nanomagnetite-nanohematite composite. J Nucl Mater 467:512–518
20. Sengupta P, Dudwadkar NL, Vishwanadh B, Pulhani V, Rao R, Tripathi SC, Dey GK (2014) Uptake of hazardous radionuclides within layered chalcogenide for environmental protection. J Hazard Mater 266:94–101
21. Baker A, Mockler NJ, Barnes WL (1999) Fluorescence intensity variations of speleothem-forming goundwaters: implications for palaeoclime reconstruction. Water Res 35:407–413
22. Genty D, Baker A, Vokal B (2001) Intra- and inter-annual growth rate of modern stalagmites. Chem Geol 176:191–212
23. Kuczumow A, Genty D, Chevallier P, Nowak J, Florek M, Buczynska A (2005) X-ray and electron microprobe investigation of the speleothems from Godarville tunnel. X-ray Spect 34:502–508
24. Pflitsch A, Holmgren D (2014) Climate study in an abandoned auto tunnel in Alaska, USA, International workshop on Ice Caves VI, proceedings of NCKRI symposium, pp.77–81
25. Webster JW, Brook GA, Railsback LB, Cheng H, Edwards RL, Alexander C, Reeder PP (2007) Stalagmite evidence from Belize

indicating significant droughts at the time of preclassic abandonment, the Maya Hiatus, and the classic Maya collapse. Palaeogeogr Palaeoclimatol Palaeocol 250:1–17
26. Boles JR (2004) Rapid growth of meter scale calcite speleothems in Mission Tunnel, Santa Barbara, CA. Water-rock interaction, Wanty, Seal II (eds), Taylor and Francis Group, London, pp. 353–356
27. Serrano MJG, Salazar PA, Sanz LFA, Jimenez YJBG (2008) Fracture sealing by mineral precipitation in a Deep Geological Nuclear Waste Repository. Rev de la Socied Espanola de Miner 9:119–120
28. Gimeno MJ, Auque LF, Acero P, Gomez JB (2014) Hydrogeochemical characterization and modeling of groundwater in a potential geological repository for spent nuclear fuel in crystalline rocks (Laxemar, Sweden). Appl Geochem 45:50–71
29. Quade J, Cerling TE (1990) Stable isotopic evidence for a pedogenic origin of carbonates in Trench 14 near Yucca Mountain, Nevada. Science 250:1549–1552
30. Alvarez NO, Glaz L, Dmowski K, Ostrega BK (2014) Mobility of toxic elements in carbonate sediments from a mining area in Poland. Environ Chem Lett 12:435–441
31. Mallampati SR, Mitoma Y, Okuda T, Sakita S, Kakeda M (2012) High immobilization of soil cesium using ball milling with nanometallic Ca/CaO/NaH_2PO_4: implications for the remediation of radioactive soils. Environ Chem Lett 10:201–207
32. Sengupta P, Sanwal J, Dudwadkar NL, Tripathi SC, Gandhi PM (2016) Adsorption of actinides within speleothem. Min Mag 80:765–780
33. Sanwal J, Dudwadkar NL, Tripathi SC, Gandhi PM, Sengupta P (2016) Adsorption of ^{106}Ru, ^{144}Ce and $^{152+154}$Eu within natural calcium carbonates and its relevance in nuclear waste disposal. J Radioanal Nucl Chem 309:751–760
34. Arcos D, Grandia F, Domenech C, Fernandez AM, Villar MV, Muurinen A, Carlsson T, Sellin P, Hernan P (2008) Long term geochemical evolution of the near field repository: insights from reactive transport modeling and experimental evidences. J Cont Hydro 102:196–209
35. Curti E (1999) Coprecipitation of radionuclides with calcite: estimation of partition coefficients based on a review of laboratory investigations and geochemical data. Appl Geochem 14:433–445
36. Nicot JP (2008) Methodology for bounding calculation of nuclear criticality of fissile material accumulations external to a waste container at Yucca Mountain, Nevada. Appl Geochem 23:2065–2081
37. Steefel CI, Lichtner PC (1994) Diffusion and reaction in rock matrix bordering a hyperalkaline fluid filled fracture. Geochim Cosmochim Acta 58:3595–3612
38. Ishikawa NK, Uchida S, Tagami K (2009) Radiocesium sorption behavior on illite, kaolinite, and their mixtures. Radioprotect 44:141–145
39. Wallace SH, Shaw S, Morris K, Small JS, Fuller AJ, Burke IT (2012) Effect of groundwater pH and ionic strength on strontium sorption in aquifer sediments: implications for ^{90}Sr mobility at contaminated nuclear sites. Appl Geochem 27:1482–1491
40. Seeprasert P, Yoneda M, Shimada Y, Matsui Y (2005) The sorption of cesium on Fungi cell: kinetic and isotherm study. Int J Pharm Med Bio Sci 4:110–114
41. Pors Nielsen S (2004) The biological role of strontium. Bone 35:583–588
42. Cornell RM (1992) Adsorption behavior of cesium on marl. Clay Min 27:363–371
43. Mukai H, Hirose A, Motai S, Kikuchi R, Tanoi K, Nakanishi TM, Yaita T, Kogure T (2016) Cesium adsorption/desorption behavior of clay minerals considering actual contamination conditions in Fukushima. Sci Rep 6:21543. doi:10.1038/serp21543
44. Mishra S, Sahoo SK, Bossew P, Sorimachi A, Tokonami S (2016) Vertical migration of radio-cesium derived from the Fukushima Dai-ichi Nuclear Power Plant accident in undisturbed soils of grassland and forest. J Geochem Explor 169:163–186
45. Chorover J, Choi S, Rotenberg P, Serne RJ, Rivera N, Strepka C, Thompson A, Mueller KT, O'Day PA (2008) Silicon control of strontium and cesium partitioning in hydroxide-weathered sediments. Geochim Cosmochim Acta 72:2024–2047
46. Thompson A, Steefel CI, Perdrial N, Chorever J (2010) Contaminant desorption during long term leaching of hydroxide-weathered Hanford sediments. Environ Sci Technol 44:1992–1997
47. Zachara JM, Smith SC, Liu C, McKiley JP, Serne RJ, Gassman PL (2002) Sorption of Cs^+ to micaceous subsurface sediments from the Hanford site, USA. Geochim Cosmochim Acta 66:193–211
48. Saunders JA, Toran LE (1995) Modelling of radionuclide and heavy metal sorption around low- and high-pH waste disposal sites at Oak Ridge, Tennessee. Appl Geochem 10:673–684
49. Gu BH, Wu WM, Ginder-Vogel MA, Yan H, Fields MW, Zhou J, Fendorf S, Criddle CS, Jardine PM (2005) Bioreduction of uranium in a contaminated soil column. Env Sci Tech 39:4841–4847
50. Gray J, Jones SR, Smith AD (1995) Discharges to the environment from the Sellafild site, 1951–1992. J Radiol Prot 15:99–131
51. Strand P, Brown JE, Drozhko E, Mokrov Y, Saibu B, Oughton D, Christensen GC, Amundsen I (1999) Biogeochemical behavior of Cs-137 and Sr-90 in the artificial reservoirs of Mayak PA. Russia. Sci Total Environ 241:107–116
52. Standring WJF, Oughton DH, Saibu B (2002) Potential remobilization of Cs-137, Co-60, Tc-99 and Sr-90 from contaminated Mayak sediments river and estuary environments. Environ Sci Tech 36:2330–2337
53. Hakem NL, Mahamid IA, Apps JA, Moridis GJ (2000) Sorption of cesium and strontium on Hanford soil. J Radioanal Nucl Chem 246:275–278
54. Steefel CI, Carroll S, Zhao P, Roberts S (2003) Cesium migration in Hanford sediment: a multisite cation exchange model based on laboratory transport experiments. J Contam Hydrol 67:219–246
55. de Konig A, Konoplev AV, Comans RNJ (2007) Measuring the specific cesium sorption capacity of soils, sediments and clay minerals. Appl Geochem 22:219–229
56. Papelis C (2001) Cation and anion sorption on granite from the Project Shoal Test site, near Fallon, Nevada, USA. Adv Environ Res 5:151–166
57. Tsai SC, Wang TH, Li MH, Wei YY, Teng SP (2009) Cesium adsorption and distribution onto crushed granite under different physiochemical conditions. J Hazard Mater 161:854–861
58. Fuller AJ, Shaw S, Peacock CL, Trivedi D, Small JS, Abrahamsen LG, Burke IT (2014) Ionic strength and pH dependent multi-site sorption of Cs onto a micaceous aquifer sediment. Appl Geochem 40:32–42
59. Kyllönen J, Hakanen M, Lindberg A, Harjula R, Vehkamäki M, Letho J (2014) Modeling of cesium sorption using cation exchange selectivity coefficients. Radiochim Acta 102:919–929
60. Hoch AR, Baston GMN, Glasser FP, Hunter FMI, Smith V (2012) Modelling evolution in the near field of a cementitious repository. Min Mag 76:3055–3069
61. Sanwal J, Kotlia BS, Rajendran CP, Ahmad SM, Rajendran K, Sandiford M (2013) Climatic variability in Central Indian Himalaya during the last $\sim$1800 years: evidence from a high resolution speleothem record. Quater Int 304:183–192
62. Chitnis RT, Rajappan SV, Kumar SV, Nadkarni MN (1979) Cation exchange separation of uranium and thorium; report BARC-1003. Bhabha Atomic Research Centre, Mumbai
63. Chen L, Xu J, Hu J (2013) Removal of U(VI) from aqueous solutions by using attapulgite/iron oxide magnetic nanocomposites. J Radioanal Nucl Chem 297:97–105

64. Chen CL, Wang XK, Nagatsu M (2009) Europium adsorption on multiwall carbon nanotube/iron oxide magnetic composite in the presence of polyacrylic acid. Environ Sci Technol 43:2362–2367
65. Fan QH, Tan XL, Li JX, Wang XK, Wu WS, Montavon G (2009) Sorption of Eu(III) on Attapulgite studied by batch, XPS, and EXAFS techniques. Environ Sci Technol 43:5776–5782
66. Mingming W, Hongqin X, Liqiang T, Jun Q, Xingquan T, Cuiping W (2012) Uptake properties of Eu(III) on Na-attapulgite as a function of pH, ionic strength and temperature. J Radioanal Nucl Chem 292:763–770
67. Lu S, Chen L, Dong Y, Chen Y (2011) Adsorption of Eu(III) on iron oxide/multiwalled carbon nanotube magnetic composites. J Radioanal Nucl Chem 288:587–593
68. Lu S, Bin M, Shuo W, Zhou J, Wang X (2015) Comparison sorption properties of Eu(III) on titanate nanotubes and rutile studied by batch technique. J Radioanal Nucl Chem 306:527–534
69. Song W, Wang X, Wang Q, Shao D, Wang X (2015) Plasma-induced grafting of polyacrylamide on grapheme oxide nanosheets for simultaneous removal of radionuclides. Phys Chem Chem Phys 17:398–406
70. Sun Y, Li J, Wang X (2014) The retention of uranium and europium onto sepiolite investigated by macroscopic, spectroscopic and modeling techniques. Geochim Cosmochim Acta 140:621–643
71. Tan X, Fan Q, Wang X, Grambow B (2009) Eu(III) sorption to TiO_2 (anatase and rutile): batch, XPS, and EXAFS studies. Environ Sci Technol 43:3115–3121
72. Yang S, Sheng G, Montavon G, Guo Z, Tan X, Grambow B, Wang X (2013) Investigation of Eu(III) immobilization on γ-Al_2O_3 surfaces by combining batch technique and EXAFS analyses: role of contact time and humic acid. Geochim Cosmochim Acta 121:84–104
73. Wang X, Li J, Dai S, Hayat T, Alsaedi A, Wang X (2015) Interactions of Eu(III) and ^{243}Am(III) with humic acid-bound γ-Al_2O_3 studied using batch and kinetic dissociation techniques. Chem Eng J 273:588–594
74. Wang X, Lu S, Chen L, Li J, Dai S, Wang X (2015) Efficient removal of Eu(III) from aqueous solutions using super-adsorbent of bentonite-polyacrylamide composites. J Radioanal Nucl Chem 306:497–505
75. Wang X, Lu S, Liu M (2015) Effect of environmental conditions on the sorption of radiocobalt on titanate/grapheme oxide composites. J Radioanal Nucl Chem 303:2391–2398
76. Chada VGR, Hausner DB, Strongin DR, Rouff AA, Reeder RJ (2005) Diavalent Cd and Pb uptake on calcite [104] cleavage faces: an XPS and AFM study. J Colloid Interface Sci 288:350–360
77. Ishikawa M, Ichikuni M (1984) Uptake of sodium and potassium by calcite. Chem Geol 42:137–146
78. Stipp SL, Hochella MF, Parks GA, Leckie JO (1992) Cd^{2+} uptake by calcite, Solid state diffusion, and the formation of solid–solution interface processes observed with near surface sensitive techniques (XPS, LEED and AES). Geochim Cosmochim Acta 56:1941–1954
79. Ricci M, Spijker P, Stellacci F, Molinari JF, Voitchovsky K (2013) Direct visualization of single ions in the stern layer of calcite. Langmuir 29:2207–2216
80. Careche M, Herrero AM, Carmona P (2002) Raman analysis of white spots appearing in the shell of Argentine red shrimp (*Pleoticus muelleri*) during frozen storage. J Food Sci 67:2892–2895
81. Mikkelsen A, Andersen AB, Engelsen SB, Hansen HCB, Larsen O, Skibsted LH (1999) Presence and dehydration of ikaite, calcium carbonate hexahydrate, in frozen shrimp shell. J Agri Food Chem 47:911–917
82. Fairchild IJ, Baker Andy (2012) Speleothem science: from process to past environments. Wiley, Hoboken, p 450
83. Sturchio M, Antonio L, Soderholm S, Sutton J (1998) Tetravalent uranium in calcite. Science 281:971–973
84. Zhong S, Mucci A (1995) Partitioning of rare earth elements (REEs) between calcite and seawater solutions at 25°C and 1 atm, and high dissolved REE concentrations. Geochim Cosmochim Acta 59:443–453
85. Cappellen PV, Charlet L, Stumm W, Wersin P (1993) A surface complexation model of the carbonate mineral-aqueous solution interface. Geochim Cosmochim Acta 57:3505–3518
86. Hoffmann S, Voitchovsky K, Spijker P, Schmidt M, Stumpf T (2016) Visualising the molecular alteration of the calcite (104)—water interface by sodium nitrate. Sci Rep 6:21576. doi:10.1038/serp21576